

MIT Open Access Articles

*Enhancing the Thermoelectric Power
Factor by Using Invisible Dopants*

The MIT Faculty has made this article openly available. **Please share** how this access benefits you. Your story matters.

Citation: Zebarjadi, Mona, Bolin Liao, Keivan Esfarjani, Mildred Dresselhaus, and Gang Chen. "Enhancing the Thermoelectric Power Factor by Using Invisible Dopants." *Advanced Materials* 25, no. 11 (March 20, 2013): 1577–1582.

As Published: <http://dx.doi.org/10.1002/adma.201204802>

Publisher: John Wiley & Sons, Inc

Persistent URL: <http://hdl.handle.net/1721.1/87019>

Version: Original manuscript: author's manuscript prior to formal peer review

Terms of use: Creative Commons Attribution-Noncommercial-Share Alike



Enhancing the thermoelectric power factor by using invisible dopants

By *Mona Zebarjadi^{#,*}, Bolin Liao[#], Keivan Esfarjani, Mildred Dresselhaus and Gang Chen^{*}*

[#] These authors contributed equally to this work.

Dr. M. Zebarjadi, B. Liao, Dr. K. Esfarjani and Prof. G. Chen

Department of Mechanical Engineering, MIT, Cambridge, 02139 Massachusetts, (USA)

Dr. M. Zebarjadi and Dr. K. Esfarjani

Department of Mechanical Engineering, Rutgers Univ., Piscataway, 08854 NJ, (USA)

E-mail: ((gchen2@mit.edu; mz270@rci.rutgers.edu))

Prof. M. S. Dresselhaus

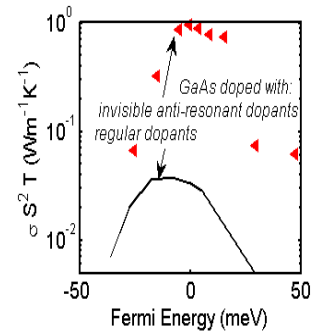
Departments of Physics and Electrical Engineering and Computer Science, MIT, Cambridge, 02139 Massachusetts, (USA)

Keywords: ((Electrical transport, Thermoelectrics, Anti-resonance scattering, Nanocomposites))

((Thermoelectric materials are usually heavily-doped with impurity

atoms to provide the required high concentration of carriers for good thermoelectric performance. These impurity atoms scatter the conduction carriers and limit their mobility. In this work we demonstrate the possibility of replacing traditional dopants with carrier-donating nanoparticles, which are invisible to the conduction

carriers in the sense that they minimally scatter conduction carriers, thus removing the deleterious effect of doping. We demonstrate that the conduction carrier scattering rate of properly designed core-shell nanoparticles, exhibit a sharp dip versus carrier energy (anti-resonant scattering). These so called anti-resonant dopants are invisible to the conduction carriers when the Fermi level is located within the dip. In addition, such a sharp minimum in the scattering cross section increases the slope of the differential conductivity ($v_g^2 \tau g(\epsilon)$) with respect to energy, and could result in the enhancement of the Seebeck coefficient. Simultaneous increase of the slope of the differential conductivity and the carrier mobility results in a large enhancement of the thermoelectric power factor (σS^2). We report more than



an order of magnitude enhancement in the thermoelectric power factor of GaAs at T=50K by replacing regular dopants with invisible anti-resonant dopants.))

1. Introduction

Increasing the efficiency of the thermoelectric energy conversion and the value of the materials' dimensionless figure of merit, $ZT = \sigma S^2 T / \kappa$, has been a major goal in energy research in the past decade, where σ is the electrical conductivity, S the Seebeck coefficient, T the temperature and κ the thermal conductivity. These properties are often interrelated which constrains the optimization of each factor and of ZT . For example, a high electrical conductivity usually leads to a low Seebeck coefficient and a high electronic contribution to a high thermal conductivity, both of which are undesirable for thermoelectric applications.

Over the past two decades, new strategies emerged on engineering electrons and phonons to increase ZT ^[1,2] such as through increased benefits from electron quantum confinement ^[3] and from phonon scattering in nanostructures ^[4]. The lattice thermal conductivity reduction has been demonstrated in many nanostructured thermoelectric materials ^[5]. However, enhancement of the thermoelectric power factor or the electronic part of ZT remains a challenge. Mahan and Sofo^[6] showed that a delta function shaped differential conductivity ($v_g^2 \tau g(\epsilon)$) as a function of energy (ϵ) results in the optimum electronic ZT . Such a delta function can either come from the density of states ($g(\epsilon)$) which will also be reflected in the group velocities ($v_g(\epsilon)$)^[7] or from the relaxation time ($\tau(\epsilon)$)^[8] of the carriers. Recently, it has been proposed that there is an optimal electronic bandwidth for each material model ^[9]. The optimal density of states has also been discussed in multi-valley semiconductors and molecular thermoelectrics ^[10]. All these works confirm the idea that incorporating sharp features in the differential conductivity will increase the thermoelectric power factor (σS^2). In particular, it has been demonstrated that resonance in the scattering rates can increase the thermoelectric power factor by enhancing the Seebeck coefficient ^[8,11]. However, such peaks in the scattering rates result in a lowering of the electrical conductivity, which is undesirable for thermoelectric performance.

In this paper, we introduce a novel strategy to design special dopants for a given semiconductor to enhance its thermoelectric performance compared to the traditional dopants. The idea is to use the freedom of design to create dopants in a way that the electron scattering cross section off of the designed dopants exhibits a sharp dip versus energy and that the sharp dip lays within the Fermi window. We refer to a sharp dip in the scattering cross section function versus carrier energy as *anti-resonant* scattering. We will show that such an anti-

resonant feature can enhance the thermoelectric performance in two different ways. First, such dopants are invisible to the conduction carriers in the sense that their interaction scattering cross section with the conduction carriers is minimal (100 times lower than the geometrical limit). Thus anti-resonant doping provides the required high concentration of carriers without scattering them and therefore removes the deleterious effect of conventional doping, and enhances the electrical conductivity (σ). Second, the sharp scattering dip would result in sharp features in the relaxation times and therefore in the differential conductivity. Therefore similar to Mahan and Sofo's work^[6], the Seebeck coefficient (S) is enhanced.

To create such anti-resonances, we get inspiration from the Ramsauer-Townsend (RT) effect^[12]. Ramsauer and Townsend observed that for slow-moving electrons in noble gases, such as argon, krypton, or xenon, the probability of collision between the electrons and gas atoms shows a minimum value for electrons with a certain amount of kinetic energy (about 0.7 eV for xenon gas). Here we investigate the feasibility of observing a corresponding anti-resonance effect in solids. One example of such a realization, as we will later show, is to embed spherically symmetric core-shell particles of appropriate size, effective mass and band offset inside a thermoelectric semiconductor. We expect that incorporation of such nanoparticles will not negatively impact the lattice thermal conductivity, κ_{ph} . In fact, we expect to observe an actual thermal conductivity reduction when there is a large acoustic mismatch between the core-shell and the host matrix materials. Therefore, the anti-resonance strategy applied to the nanoparticle-doped samples points to a direction that can be used to improve the three parameters determining the figure of merit (σ , S and κ) over that for both impurity-doped and traditional nanoparticle-doped samples. We would like to point out that the anti-resonance scattering concept that we are introducing here has applications much wider than the thermoelectrics field. In fact, the concept could be applied to the materials design of any semiconductor device for which high carrier mobility is desired. This concept can be considered as an alternative to modulation-doping^[13] which is widely used in microelectronics and photonic devices.

In this paper we first discuss the possibility of creating these anti-resonance features in the scattering cross section of electrons off of dopants. That is the equivalent of the Ramsauer-Townsend effect in solids. Then we demonstrate the enhancement in the thermoelectric power factor by replacing the traditional dopants with the anti-resonant nanoparticle dopants. Finally we discuss the advantages and the applications of the proposed strategy.

2. Extension of Ramsauer-Townsend effect to solids (anti-resonance scattering):

By engineering the electron scattering rates ($1/\tau(\varepsilon)$), one can increase the thermoelectric power factor. An example of such engineering is in samples in which ionized impurity scattering is the dominant scattering mechanism. In such samples, ionized impurities can be replaced by proper ionized nanoparticles. Since nanoparticles have more degrees of freedom (including nanoparticle size, shape, height of the potential barrier $V(r)$, the charge carrier concentration, volume fraction and effective mass), there is more room to optimize the power factor using nanoparticles compared to single impurities. As a result, nanoparticle-doped samples have been demonstrated to be advantageous compared to impurity-doped samples in several cases^[14-17]. However, in most cases, these nanoparticles are simple one layer spheres, and they become scattering centers that can limit the electrical conductivity increase. Suppose that we can use the freedom of design to fabricate nanoparticles with a specific radial potential function profile to minimize the electron scattering cross section (Σ) within the Fermi window ($E_f \pm k_B T$) to guarantee mobility enhancement. At the same time, if the scattering cross section ($\Sigma \propto 1/\tau$) versus energy has a large slope close to the Fermi level (E_f), the Seebeck coefficient (S), which is roughly proportional to the slope of the logarithm of the differential conductivity ($\sigma(\varepsilon) = v_g^2 \tau g(\varepsilon)$), will also be enhanced (**Eq. 1-Mott Formula**^[18]).

$$S = -\frac{\pi^2}{3} \frac{k_B^2 T}{e} \left. \frac{d \log \sigma(\varepsilon)}{d\varepsilon} \right|_{\varepsilon=E_f}. \quad (1)$$

This in nature is similar to the Ramsauer-Townsend observed minimum in the scattering cross section of the electrons off of rare gas atoms. Physically, the Ramsauer-Townsend effect may be thought of as a diffraction of the electron around the rare-gas atom, in which the wave function inside the atom is distorted in such a way that it fits on smoothly to an undistorted wave function outside the atom^[19]. The Ramsauer-Townsend effect is analogous to the perfect transmission found at particular energies in the one-dimensional carrier scattering from a potential well. Mathematically, the Ramsauer-Townsend effect can be explained using the partial wave method. This method is the exact solution for the electron scattering from a single spherically symmetric potential. Using this technique, the total scattering cross section is written as a sum over partial waves with angular momentum l values ranging from zero to infinity:

$$\Sigma = \frac{4\pi}{k^2} \sum_{l=0}^{\infty} (2l + 1) \sin^2 \delta_l . \quad (2)$$

Each partial wave (φ_l) has a phase shift (δ_l), relative to the incoming wave. If the phase shift is zero or a multiple of π , the scattered wave looks the same as the incoming wave. In this case, the potential is “screened” and there is no observable difference between the incoming and the outgoing wave, which is as if there is no scattering center. Since there are an infinite number of partial waves (φ_l), it is impossible to set all phase shifts to zero at a given energy. However, for an electron of angular momentum $\hbar l$ and momentum $\hbar k$, the impact parameter is $\frac{\hbar l}{\hbar k} = \frac{l}{k}$ and when the impact parameter is larger than the range of the potential, a , or ($l > ka$), then the scattering will be weak. Therefore, only l values smaller than ka are contributing dominantly to the cross section sum (**Eq. 2**).

At low enough energies, only the $l = 0$ and $l = 1$ terms in Eq. 2 contribute, and we can try to make the two corresponding phase shifts to become a multiple of π to make the cross section vanish. To achieve this, we adopt a core-shell structure with six parameters: the inner and outer radii of the scattering core-shell structure, the corresponding band offset and the effective mass. The coexistence of a barrier and a potential well plays the key role. While a potential well pulls in the partial waves towards the origin, a potential barrier pushes them out. By controlling the amplitude of the barrier and the well appropriately in a core-shell structure, the effect of the two can be cancelled out for each partial wave at a different energy. If the cancelation energies of the 0th and 1st order partial wave are very close to each other and when ka is smaller than one ($ka < 1$), then a sharp minimum is observable in the total scattering cross section as shown in **Fig. 1**. A more detailed discussion and the role of the different parameters in the design of the potential function is presented in a separate publication ^[20].

Figure 1 demonstrates that it is possible to design dopants with anti-resonant features in analogy to the Ramsauer-Townsend observation but for ionized particles in solids. For the given core-shell structure which is shown in Fig. 1a, the calculated electron scattering cross section indicates a sharp minimum value as shown in Fig. 1b. Details of the modeling, including solving the Poisson equation within the Thomas-Fermi approximation to obtain the appropriate screened bent potential, the calculation of the wave function inside the nanoparticles and finally the scattering cross section are all provided in the supporting information. The parameters for the designed core-shell structure are reported in **Table 1**.

Figure 1 is plotted for the $z=1$ nanoparticle (z is the number of carriers per nanoparticle) reported in Table 1.

For carriers of energies close to the minimum (about 27meV in Fig. 1b), the nanoparticles are invisible meaning that electrons pass through these nanoparticles almost with no scattering. We would like to emphasize that the set of parameters that is reported here is only an example and is not unique. There is a great flexibility of design since there are many adjustable parameters and such anti-resonances could be easily identified by looking at the roots of different l components. For example, for the reported set of parameters as we increase the barrier height, the position of the minimum shifts to higher energies and as we increase the bending of the potential (by means of increasing the number of donated electrons per nanoparticle or decreasing the screening length), the minimum shifts to lower energies. All three sets of parameters reported in Table 1 result in a similar scattering cross section (Σ) to that reported in Fig. 1.

3. Demonstration of the enhanced power factor

In this section, we demonstrate that by replacing the traditional impurity dopants with the designed anti-resonant dopants or the invisible dopants, we can greatly enhance the thermoelectric performance. It is important to note that the proposed strategy is most effective when applied to the samples in which the electron scattering from dopants is the dominant scattering mechanism for the carrier transport, e.g. at low temperatures and for defect-free crystals. We have previously shown that 3D modulation-doped samples have a better performance compared to uniformly-doped samples because of the reduced impurity scattering and therefore enhanced carrier mobility ^[21]. For the modulation-doping strategy, ionized nanoparticles are concentrated inside nanoparticles and the host matrix is left undoped ^[22]. Charge carriers are then transferred from the nanoparticles into the host matrix, leaving their parent atoms behind inside the nanoparticles, which results in a reduced carrier-impurity scattering. Using such a strategy, in the actual experiment, only a 40% improvement in the carrier mobility has been demonstrated ^[21]. This enhancement is significant but not ideal. The reason for the limited improvement is the competition between the impurity scattering and the nanoparticle scattering. In fact, in the modulation-doped samples ^[21], the impurity scattering is replaced by the nanoparticle scattering, which is demonstrated to be weaker. Now if we can shield the nanoparticles and make them invisible, then a much higher improvement in the mobility would be expected. Therefore, by combining the anti-resonance scattering with the modulation-doping strategy, we can improve the mobility by minimizing the nanoparticle

scattering at energies close to the Fermi-level and by making the nanoparticles as invisible as possible to the conducting electrons. In this sense, the applications of the anti-resonance strategy go beyond the thermoelectric field and could be applied whenever high electrical conductivity is required in semiconductor devices.

In the thermoelectrics field, anti-resonance scattering is most useful since the sharp features in the anti-resonance scattering rates also increase the Seebeck coefficient. Finally even though the nanoparticles are invisible to the electrons, they can reduce the phonon thermal conductivity significantly if there is a large acoustic mismatch between the core-shell nanoparticles and the host matrix.

For the purpose of illustration, we choose GaAs as the host material. The GaAs materials properties and transport properties are well known and there exist available experimental data as well as theoretical models for this test material. The important carrier scattering rates of GaAs are calculated based on the standard developed formalisms^[23] and are plotted in **Fig. 2** for a low temperature of 50K. The materials parameters are reported in the supporting information and they reproduce well experimental data for the electron mobility. The impurity dopants reported in the plot are calculated at the optimum Fermi level of the impurity doped sample. The idea here is to replace the impurity dopants with anti-resonant nanoparticle dopants so as to increase ZT. Once we know the relative strengths of the impurity scattering and the phonon scattering, we can design the anti-resonant nanoparticle scattering in a way to increase the mobility and to increase the Seebeck coefficient at the same time. As mentioned before, there is a lot of flexibility in the design of anti-resonant nanoparticles and we can tune the strength of the scattering rate. For the three sets of parameters reported in Table 1, the scattering cross section is similar and is reported in Fig. 1b. However, to obtain a similar level of charge carrier density, a lower volume fraction of more charged nanoparticles is required. Therefore, for the same Fermi level, the scattering rate of nanoparticles with $\beta = 2$ is lower than that for nanoparticles with $\beta = 1$. In addition an arbitrary amount of neutral nanoparticles could always be added to increase the scattering rate. Therefore, it is relatively easy to tune the scattering rate of the designed nanoparticles.

A lower scattering rate enhances the mobility. However, if the scattering rate is too low, then its sharp features are affected by the background phonon scattering. We then need to increase the amplitude of the scattering, so that the sharp features are visible and result in the enhanced Seebeck coefficient. Figure 2 shows two different scattering rates which are calculated from two different designed nanoparticles (with different β parameters). The main difference between the two rates is their scattering amplitude; otherwise they have similar

features. As one can see from Fig. 2, the np2 set of dopants ($\beta=2$), show a weaker scattering rate (which is desirable for having a higher carrier mobility) but in the energy range where the sharp dip exists, the phonon scattering rates are dominant and therefore the Seebeck coefficient is not expected to increase. On the other hand, the np1 set of dopants ($\beta=0.1$, note that this is the average charge per nanoparticle as in this case there is a combination of neutral nanoparticles as well as nanoparticles donating one electron) is expected to enhance the Seebeck coefficient while only moderately increasing the mobility.

Figure 3 illustrates the power factor enhancement for the suggested nanoparticle design. The power factor is compared with the impurity-doped sample and the traditional nanoparticle-doped samples. In order to increase the carrier concentration and therefore the Fermi-level, we need to increase the volume fraction of the nanoparticles. We did not increase the volume fraction beyond 10% as the current formalism (partial wave) is only valid in the dilute limit and here we did not include the multiple scattering effects and the band structure modifications of the host matrix as a result of high doping concentration, even though such effects might lead to further enhancements in the power factor^[16]. As shown in Fig. 3, both types of nanoparticles (np1 and np2) reported in Fig. 2, can enhance the power factor. The first set (np1) results in the simultaneous enhancement of the Seebeck coefficient and the electrical conductivity as the minimum in the momentum scattering rate is very sharp and the scattering rate is lower compared to the impurity scattering rate. The second set (np2) benefits only from a very large mobility enhancement but the Seebeck coefficient is almost the same as the impurity doped sample since the background phonons are dominant within the dip energy range. For the studied case, as can be seen in Fig. 3, the second set results in a higher increase of the power factor. That is, for the sample under study, it is more beneficial to the power factor to sacrifice the increase in Seebeck coefficient to obtain a much better mobility. Nevertheless, we showed that it is possible to simultaneously enhance the Seebeck coefficient and the electrical conductivity and it is also possible to make the dopants as invisible as desired to enhance the mobility largely.

Let us focus on the np2 set of nanoparticles and only focus on enhancing the mobility. The thermoelectric power factor of the np2 nanoparticle-doped sample is an order of magnitude higher than the impurity-doped sample which is mainly the result of enhancement in the carrier mobility (Fig. 3). We know that even by traditional nanoparticle doping (modulation-doping) the carrier mobility is enhanced which raises the question of how much of the observed enhancement is coming from the shielding of the nanoparticles and how much of it is coming from the traditional nanoparticle doping. To answer this question, we take off the

shell of the np2 nanoparticles and calculate the transport properties of a sample doped with these new nanoparticles. The results are reported in Fig. 3 and are labeled with npt for traditional nanoparticles. Figure 3 indicates that the modulation-doped sample (or traditional nanoparticle-doped sample) has a thermoelectric power factor which is only about 50% higher than the impurity doped samples, therefore the remaining enhancement in the thermoelectric power factor comes from the shielding of the nanoparticles which highlights the effectiveness of the proposed strategy.

3.1. Effect of temperature and the sensitivity on the parameters

As the temperature increases, we reach the regime where phonon scattering is dominant. In this limit, the strategy is less effective since the impurity scattering becomes relatively less important. Furthermore, when the Fermi-window ($k_B T$) is wider, the sharp features in the scattering rates are washed out in the linearized Boltzmann integrals, and therefore the loss of the sharp features results in a lower Seebeck coefficient.

For the designed nanoparticles of Table 1, we noted that the enhancement in the power factor decreases as we increase the temperature above $T=50\text{K}$ and there are no observable enhancements found above room temperature. The huge enhancement reported in Fig. 3 for the thermoelectric power factor (reported for $T=50\text{K}$) is slightly lower when we increase the temperature to $T=100\text{K}$. This is reported in the **Fig. S2** of the supporting information.

We have also noted that the second set of anti-resonant nanoparticles (np2) which only enhance the mobility and not the Seebeck coefficient is less sensitive to the randomness of the system. That is the enhancement in the power factor is observable even if there are fluctuations in the practical realization of the individual parameters. But the first set of anti-resonant nanoparticles (np1) is largely sensitive to such fluctuations. The reason is that the first set is largely benefitting from the sharp features of the scattering rates. When there is randomness in the system, such fluctuating features are suppressed on average and there is no enhancement in the Seebeck coefficient. In the supporting information we have included some of the sensitivity analysis.

4. Summary and conclusions:

We conclude that the concept of the Ramsauer-Townsend anti-resonance, when applied to a thermoelectric material, allows the simultaneous enhancement of the electrical conductivity and the Seebeck coefficient. In the present studied case, invisibility of the dopants seemed to be more important than the sharp features in the differential conductivity. We are not making

any claims concerning the transport values that might be obtained quantitatively. The GaAs material is not an especially favorable low-temperature thermoelectric material. The designed core-shell nanoparticle also is not the optimized nanoparticle profile but just one, among the many possibilities, which give rise to anti-resonance behavior. The core-shell structure is the simplest structure that we could use for the demonstration purpose. More complicated structures can be used to demonstrate the same effect. The GaAs host matrix with the incorporated core-shell nanoparticles is used in the present work only as an example to illustrate the thermoelectric enhancement as a result of using anti-resonant dopants. We have not yet done a full optimization of the parameters to maximize the thermoelectric power factor. However, even without optimization, more than an order of magnitude enhancement in the power factor is obtained. The calculated potential profile contains the essential physics of the charge transport process including the charge transfer and the screening effects. The starting two-step potential is an effective potential in the presence of bound states and is not purely the band offset between two dissimilar materials. A complete study of specific materials for the nanoparticles as well as the host matrix will be the subject of a future research.

To summarize, we introduced the concept of anti-resonance scattering to enhance the power factor of thermoelectric materials. This approach is most useful at low temperatures and when the free carriers come from the nanoparticles. We showed that it is possible to design ionized core-shell nanoparticles with anti-resonant features in their electron scattering cross section, making these nanoparticles invisible to the conduction electrons. Embedding such nanoparticles in semiconductor matrices can enhance both the electrical conductivity and the Seebeck coefficient simultaneously. Furthermore, a thermal conductivity reduction is also expected when there is a large acoustic mismatch between the core-shell and the host matrix. In this sense, we can expect to simultaneously improve all three parameters that are relevant to determining ZT , thus representing an advance over traditional impurity-doped and nanoparticle-doped samples. In the current study more than an order of magnitude enhancement in the thermoelectric power factor was observed by using invisible dopants. Ionized nanoparticles with anti-resonance features can be implemented in any materials design for which high carrier mobility is desired and this strategy could be considered as a better alternative to modulation-doping.

Acknowledgements

This article is based upon work supported as part of the MIT S3TEC, an Energy Frontier Research Center funded by the U.S. Department of Energy, Office of Science, Office of Basic Energy Sciences under Award Number DE-FG02-09ER46577 (for basic research).
((Supporting Information is available online from Wiley InterScience or from the author.))

-
- [1] M. Zebarjadi, K. Esfarjani, M. S. Dresselhaus, Z. F. Ren and G. Chen, *Energy and Environ. Science*, **2012**, 5, 5147-5162.
- [2] J. R. Sootsman, D. Y. Chung and M. G. Kanatzidis, *Angew. Chem., Int. Ed.*, **2009**, 48, 8616.
- [3] L. D. Hicks and M. S. Dresselhaus, *Phys. Rev. B* **1993**, 47, 12727.
- [4] G. Chen, *Phys. Rev. B* **1998**, 57, 14958–14973.
- [5] YC. Lan, AJ. Minnich, G. Chen, ZF. Ren, *Adv. Func. Mat.*, **2010**, 20, 357.
- [6] G. D. Mahan and J. O. Sofo, *Proc. Natl. Acad. Sci. U.S.A.* **1996**, 93, 7436.
- [7] J. P. Heremans, V. Jovovic, E. S. Toberer, A. Saramat, K. Kurosaki, A. Charoenphakdee, S. Yamanaka, G. F. Snyder, *Science* **2008**, 321, 554.
- [8] Yu. I. Ravich, in *CRC Handbook of Thermoelectrics*, D. M. Rowe, Ed. (CRC Press, Boca Raton, FL, 1995), pp. 67–81.
- [9] J. Zhou, R.G. Yang, G. Chen and M. S. Dresselhaus, *Phys. Rev. Lett.*, **2011**, 107, 226601.
- [10] C. Jeong and M. Lundstrom, *J. Elect. Mat.*, **2011**, 40, 738.
- [11] J. P. Heremans, B. Weindlocha and A. M. Chamoire, *Energy and Environmental Science*, **2012**, 5, 5510.
- [12] V. A. Bailey, and J. S. Townsend, *Philosophical Magazine*, **1921**, S.6, 42, 873-891; Ramsauer, C., *Annalen der Physik*, **1921**, 4, 64, 513–540.
- [13] Daembkes, H.; 2nd Eds, *Modulation-doped Field-effect Transistors: Principles, Design, and Technology* (IEEE press, **1991**).
- [14] S. V. Faleev and F. Leonard, *Phys. Rev. B*, **2008**, 77, 214304
- [15] M. Zebarjadi, K. Esfarjani, A. Shakouri, J. Bahk, Z. X. Bian, G. Zeng, J. E. Bowers, H. Lu, J. M. O. Zide and A. C. Gossard, *Appl. Phys. Lett.*, **2009**, 94, 202105.
- [16] M. Zebarjadi, K. Esfarjani, Z. X. Bian and A. Shakouri, *Nano Lett.*, **2011**, 11, 225
- [17] J. H. Bahk, Z. X. Bian, M. Zebarjadi, P. Santhanam, R. Ram and A. Shakouri, *Appl. Phys. Lett.* **2011**, 99, 072118.
- [18] N. F. Mott and E. A. Davis, *Electronics Processes in Non-crystalline Materials* (Clarendon, Oxford, **1971**).
- [19] L. I. Schiff, *Quantum Mechanics* (McGraw-Hill, New York, **1949**).
- [20] B. Liao, M. Zebarjadi, K. Esfarjani and G. Chen, *Phys. Rev. Lett.*, **2012**, 109, 126806.
- [21] M. Zebarjadi, G. Joshi, G. H. Zhu, B. Yu, A. Minnich, Y. C. Lan, X. W. Wang, M. S. Dresselhaus, Z. F. Ren and G. Chen, *Nano Lett.*, **2011**, 11, 2225.
- [22] B. Yu, M. Zebarjadi, K. Lukas, H. Wang, C. Opeil, M. S. Dresselhaus, G. Chen and Z. F. Ren, *Nano Lett.*, **2012**, 12, 2077.
- [23] M. Lundstrom, *Fundamentals of Carrier Transport*, Cambridge University press, **2000**.

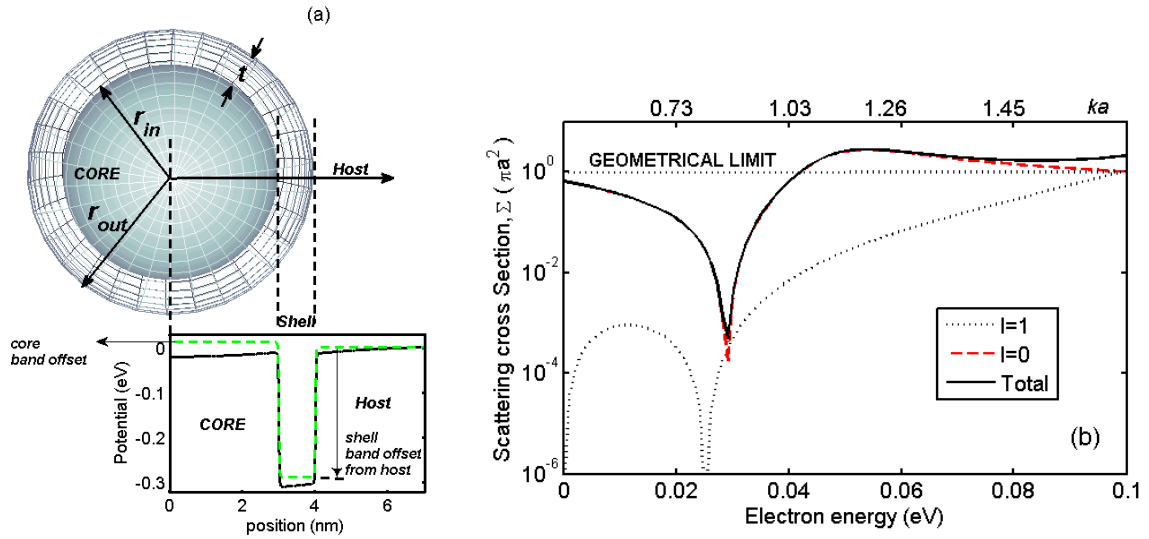


Figure 1. ((a) A cartoon of the core-shell nanoparticle. The potential profile of the nanoparticle is plotted as a function of position in the radial direction. The band offset profile across the core-shell nanoparticle is plotted with the green dashed line and the screened bent potential with the solid line. b) The total electron-nanoparticle scattering cross section versus electron energy (bottom scale) or ka (top scale) is depicted with a solid line. The contribution of the 0th order (dashed line) and the 1st order (dotted line) partial waves are also plotted. The core-shell potential parameters are summarized in Table 1. The volume fraction of the nanoparticles is 1%, the doping level is $5 \times 10^{16} \text{cm}^{-3}$, and this doping level corresponds to about 1 electron per nanoparticle.))

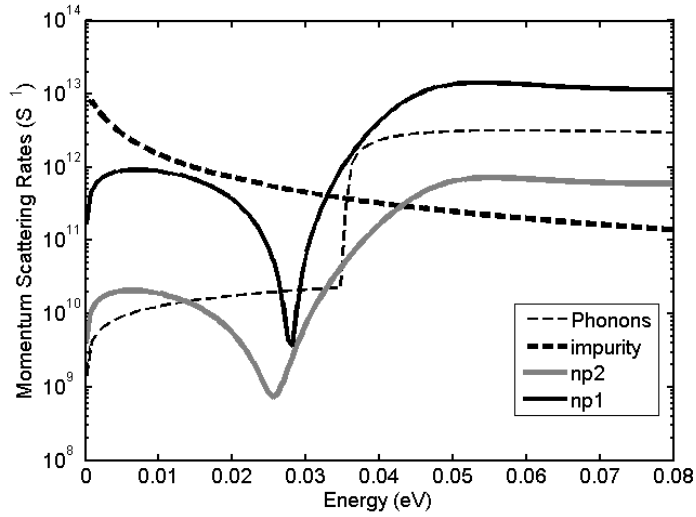


Figure 2. ((The momentum scattering rate calculated for different electron scattering mechanisms at 50K for GaAs. The phonon rates include electron scattering by polar optical and acoustic phonons. The traditional ionized impurity scattering rate (labeled as impurity) at the optimum Fermi level (-5meV) is also plotted. This latter scattering can be replaced by the proposed anti-resonant core-shell nanoparticles. Two different anti-resonant nanoparticles are used. The np1 set is a combination of neutral and $\bar{z}=1$ nanoparticles reported in Table 1. On the average $\bar{z}=0.1$ for this set. The np2 set is made of nanoparticles with $\bar{z}=2$ reported in Table 1.))

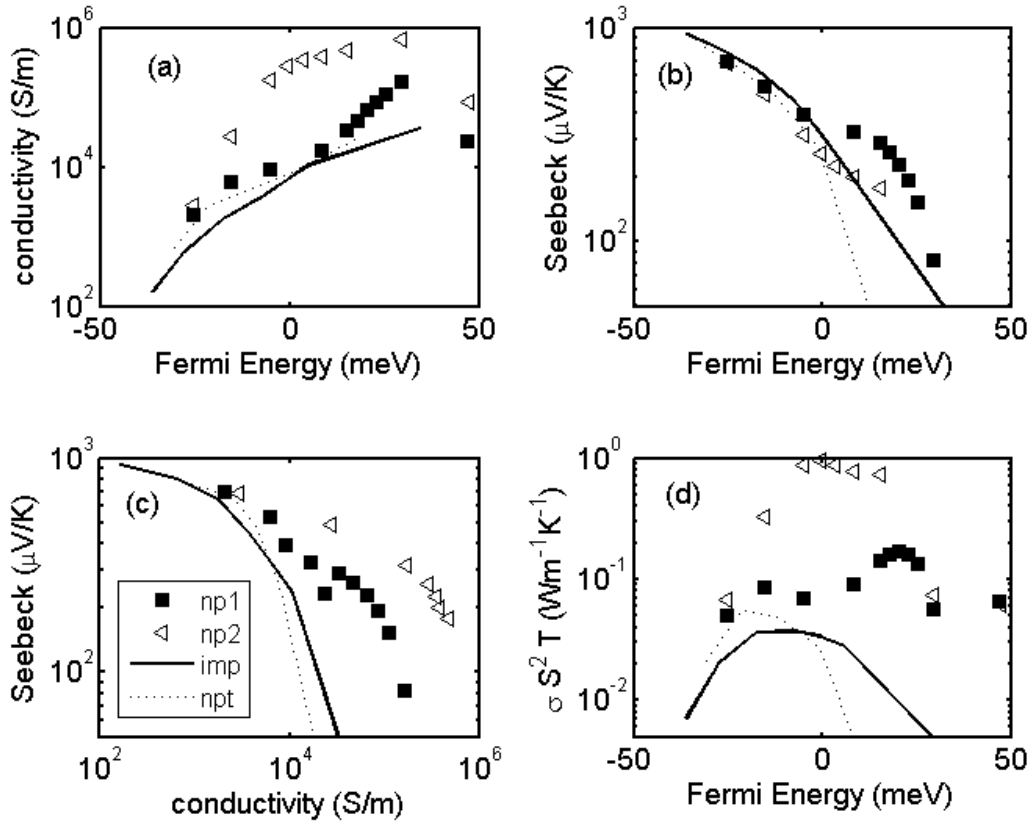


Figure 3. ((The Fermi level dependence of the electrical conductivity (a), the Seebeck coefficient (b) and the product ($\sigma S^2 T$) (d) calculated for doped GaAs at T=50K. The Seebeck coefficient as a function of the electrical conductivity (c) is also plotted. Four different types of dopants are considered: regular impurities (solid line, imp), traditional nanoparticles (dotted line, npt), and two sets of anti-resonant nanoparticles (np1 and np2 defined in the inset to Fig. 2). The considered traditional nanoparticle is a one layer nanoparticle made out of the core of the nanoparticle denoted as np2 (the $z=2$ nanoparticle of Table 1).))

Table 1. ((Parameters of the core-shell structure: The first set of parameters are reported for a neutral nanoparticle ($\mathfrak{z}=0$). For a charged nanoparticle ($\mathfrak{z}=1$ and 2) we can use the same values of the parameters and only vary the barrier height to recover a similar cross section.))

| \mathfrak{z} | Parameters | Core | Shell |
|------------------|-----------------------|------------------|-------------------|
| $\mathfrak{z}=0$ | effective mass (m) | $0.58m_0$ | $0.6m_0$ |
| | band offset from host | -30meV | -285 meV |
| | Layer size | 3nm (r_{in}) | 1nm thick (t) |
| $\mathfrak{z}=1$ | band offset from host | 11 meV | -285 meV |
| $\mathfrak{z}=2$ | band offset from host | 33meV | -285 meV |

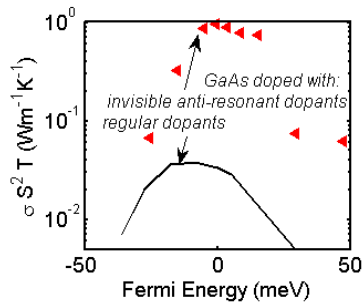
The table of contents entry: invisible anti-resonant dopants enhance the thermoelectric power factor of the heavily doped semiconductors largely over the traditional dopants.

Keyword (see list)

M. Zebarjadi, B. Liao, K. Esfarjani, M. S. Dresselhaus and G. Chen*((same order as byline))

Enhancing the thermoelectric power factor by using invisible dopants ((no stars))

ToC figure ((55 mm broad, 50 mm high, or 110 mm broad, 20 mm high))



Enhancing the thermoelectric power factor by using invisible dopants

Mona Zebarjadi, Bolin Liao, Keivan Esfarjani, Mildred Dresselhaus and Gang Chen

S1. Calculation of the scattering rate of electron-nanoparticle:

Table S1. List of Symbols

| | |
|-----------------------|--|
| Σ | Total scattering cross section |
| Σ_m | Momentum Scattering cross section |
| τ | electron relaxation time |
| μ | electron mobility |
| E_f | Fermi level |
| $\sigma(\varepsilon)$ | Differential conductivity |
| σ | Electrical conductivity |
| $g(\varepsilon)$ | Density of states |
| λ | Screening length |
| S | Seebeck coefficient |
| \mathfrak{z} | Average number of electrons per nanoparticle |
| k_B | Boltzmann constant |
| T | Temperature |

We assume that nanoparticles are spheres with a radius of r_{out} and each nanoparticle donates \mathfrak{z} electrons to the conduction band. A cartoon of this picture is shown below.

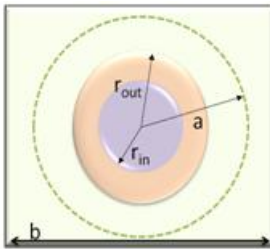


Figure S1. Cartoon of a spherically symmetric core-shell nanoparticle of radius r_{out} inside the host matrix. The square represents an area (b^2) of the host material in which only one nanoparticle on the average exists. r_{in} is the core radius and a is the potential range after which the potential of the nanoparticle is zero.

Volume fraction of nanoparticles: $V_{fr} = \frac{4\pi r_{out}^3}{3b^3}$

Density of nanoparticles: $\rho_{np} = \frac{3V_{fr}}{4\pi r_{out}^3}$

Free carrier density: $n = 3\rho_{np}$

Then the Fermi level (E_f) of the system is determined from the solution of:

$$n = \int g(\varepsilon) f(\varepsilon - E_f) d\varepsilon \quad (S1)$$

The Thomas-Fermi ($1/\lambda$) screening length is calculated from:

$$\lambda^2 = \frac{q^2}{\varepsilon} \int g(\varepsilon) \frac{\partial f}{\partial \varepsilon} d\varepsilon \quad (S2)$$

$g(\varepsilon)$ is the density of states inside the host matrix and $f(\varepsilon - \mu)$ is the Fermi-Dirac function.

The potential of the nanoparticle is calculated based on the Thomas-Fermi model of screening by solving the Poisson equation, assuming that the charge is uniformly distributed inside the nanoparticle.

$$\text{Ion charge density: } \rho_+(r) = \begin{cases} \frac{3}{4/3\pi r_{out}^3} & 0 < r < r_{out} \\ 0 & r_{out} < r \end{cases} \quad (S3)$$

According to the Thomas-Fermi approximation, the potential and the carrier density in Fourier space are related through:

$$V(q) = \frac{4\pi}{q^2 + \lambda^2} \rho(q) \quad (S4)$$

The final potential of the nanoparticle is calculated by adding the potential due to Eq. S3 and Eq. S4 and the band offsets between dissimilar materials.

Given the potential, the wave function for a given carrier energy can be calculated by solving the Schrödinger equation inside the nanoparticles. The equation for the radial part of the wave function ($R(r)$) in a spherically symmetric potential ($V(r)$) in the presence of a position dependent effective mass ($m(r)$) can be written as:

$$\frac{\partial^2 U}{\partial r^2} - \frac{l(l+1)}{r^2} + \frac{2m}{\hbar^2} (\varepsilon - V(r)) U - \frac{m'}{m} r \frac{\partial R}{\partial r} = 0; \quad U = rR \quad (S5)$$

in which l is the angular momentum quantum number. We solve Eq. S5 numerically inside the nanoparticle. At the junctions between dissimilar materials (e.g. boundary of the nanoparticle and the host and in the case of bi-layer nanoparticles, the boundary of the core and the shell) there is discontinuity of the band profile (band offset) and the effective mass. To prevent

numerical errors, we smooth the junctions by a Fermi type function with a width of about 100 mesh points corresponding to 1 Å.

From the above calculations all that is required is the slope of the wave function over its absolute value at the nanoparticle potential range ($r=a$)

$$\gamma_l = \frac{R'}{R} \Big|_{r=a} \quad ,(\text{S6})$$

The partial-wave method is then used to calculate the scattering cross-section from a spherically symmetric potential²³.

$$\Sigma(\theta) = \frac{1}{k^2} \left| \sum_{l=0}^{\infty} (2l+1) e^{i\delta_l} \sin \delta_l P(\cos \theta) \right|^2 \quad (\text{S7})$$

$$\Sigma = \frac{4\pi}{k^2} \left[\sum_{l=0}^{\infty} (2l+1) \sin^2 \delta_l \right] \quad (\text{S8})$$

$$\Sigma_m = \frac{4\pi}{k^2} \left[\sum_{l=0}^{\infty} (2l+1) \sin^2 \delta_l - \sum_{l=0}^{\infty} 2l \cos(\delta_l - \delta_{l-1}) \sin \delta_l \sin \delta_{l-1} \right] \quad (\text{S9})$$

$$\tan \delta_l = \frac{k j_l'(ka) - \gamma_l j_l(ka)}{k n_l'(ka) - \gamma_l n_l(ka)} \quad (\text{S10})$$

$$\frac{1}{\tau_m} = \sum_m v_g \rho_{np} \quad (\text{S11})$$

Here, θ is the scattering angle, $\Sigma(\theta)$ is the angular dependent cross section, Σ is the total cross section, Σ_m is the momentum cross section, τ_m is the momentum relaxation time, δ_l is the phase shift of the l th partial wave, v_g is the group velocity, k is the wave-vector and a is the particle potential radius after which the potential is zero. P_l is the Legendre function, j_l and n_l are the spherical Bessel functions of the first and second kind, respectively.

S2. Calculation of transport properties for GaAs:

We assume a single parabolic band structure and the parameters used are summarized in Table S2.

Table S2. GaAs material parameters used in the calculations

| Material Parameters: | |
|--------------------------------------|----------------------------|
| Effective mass (Γ valley) | 0.063 m_0 |
| dielectric constant (static) | 12.9 |
| dielectric constant (high frequency) | 10.89 |
| Density | 5.317 g cm ⁻³ |
| Sound velocity | 5.22 x10 ⁵ cm/s |
| Polar optical phonon energy | 0.03536 eV |
| Acoustic deformation potential | 7 eV |

Matthiessen's rule is used to add the momentum scattering rates of acoustic phonons, polar optical phonons, neutral impurities, ionized impurities and/or nanoparticles to obtain the total momentum scattering rate ($1/\tau_m$) for the impurity doped and the nanoparticle doped samples. These rates are plotted in figure 3 of the manuscript.

Linearized Boltzmann transport integrals then were used to calculate the Seebeck coefficient (S) and the electrical conductivity (σ):

$$S = \frac{1}{eT} \left(\frac{\int v^2 (\varepsilon - \mu) \tau_m(\varepsilon) g(\varepsilon) \frac{\partial f}{\partial \varepsilon} d\varepsilon}{\int v^2 \tau_m(\varepsilon) g(\varepsilon) \frac{\partial f}{\partial \varepsilon} d\varepsilon} \right) \quad (\text{S12})$$

$$\sigma = -\frac{2e^2}{3m^*} \int \varepsilon \tau_m(\varepsilon) g(\varepsilon) \frac{\partial f}{\partial \varepsilon} d\varepsilon \quad (\text{S13})$$

S3. Power factor enhancement at 100K

To illustrate the temperature dependence, here we report the results of the power factor enhancement at $T=100\text{K}$. We compare the impurity doped GaAs with the core-shell anti-resonant nanoparticle doped GaAs (np2 set of the manuscript).

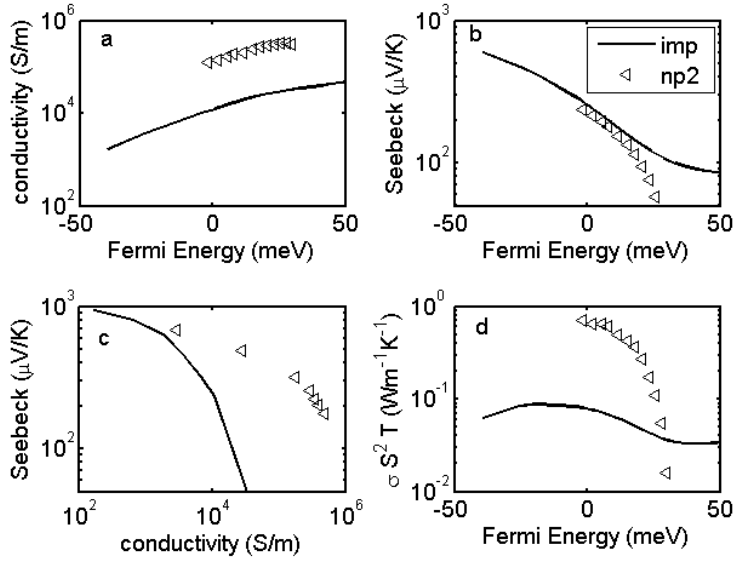


Figure S2. The electrical conductivity (a), the Seebeck coefficient (b) and the product ($\sigma S^2 T$) (d) of the impurity- doped sample (solid line), and the anti-resonant nanoparticle-doped sample (np2) versus Fermi level calculated for GaAs at 100K. np2 refers to the nanoparticle with $\beta=2$ reported in Table 1 of the manuscript.

S4. Sensitivity of the scattering rates

In an actual experimental configuration, fluctuations in the parameters are expected for different points in the sample. Here we look at fluctuations of one of the parameters, that is, the core radius. Assume that there is a Gaussian distribution for the core radius of the nanoparticles. The assumed distribution function is shown in the inset of Fig. S3.

Figure S3 top is calculated for the first set of nanoparticles reported in the paper (np1). We fix all the parameters and we change the radius of the core and calculate the scattering cross section for the same Fermi level (-5meV) reported in figure 2 of the manuscript. The scattering cross section for each radius is calculated and reported in figure S3. Then we average over these rates according to the weight of each nanoparticle radius. The average scattering rate is also plotted with a thick line. Also as a reference, the impurity scattering rate

at the same Fermi-level is plotted. We repeat the same steps for the second set of nanoparticles (np2) and report the results in figure S3, bottom. The results of the power factor calculations are summarized in Table S3. As can be seen, randomness decreases the power factor of the np1 set by about 50% and that of np2 by only 17%.

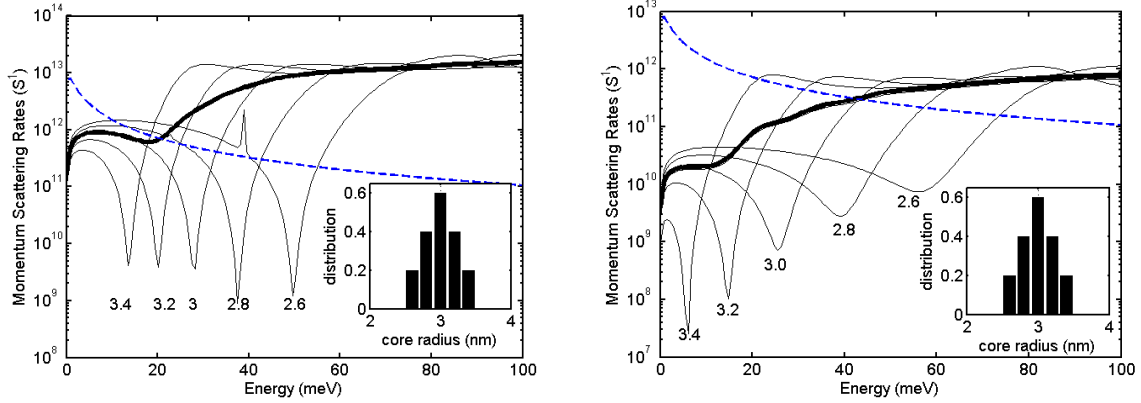


Figure S3. The momentum scattering rate calculated for nanoparticles of different core radii. All the other parameters and the carrier density are the same for these nanoparticles, and the core radii values are labeled for each nanoparticle. The left figure is calculated for the np1 set of nanoparticles and the right figure for the np2 set. Refer to the manuscript for the properties of these two sets. The dashed line shows the impurity scattering rate calculated at the same Fermi level as those of the nanoparticles (-5meV). The solid thick line is the weighted average of the nanoparticle scattering rates (see text).

Table S3- Result of calculated power factor values at 50K and at the optimum Fermi level of the impurity doped GaAs

| Power factor | W/mK^2 |
|--|----------------------|
| Impurity doped | 7.4×10^{-4} |
| np1 set with a single core radius | 4.5×10^{-3} |
| np1 set with averaging over the core radius distribution | 2.8×10^{-3} |
| np2 set with a single core radius | 1.9×10^{-2} |
| np2 set with averaging over the core radius distribution | 1.6×10^{-2} |